Use of Clement's ODEs for the speedup of computation of the Green function and its derivatives for floating of submerged bodies in deep water

Chunmei Xie, Aurélien Babarit, François Rongère, Alain H. Clément

USE OF CLEMENT'S ODES FOR THE SPEEDUP OF COMPUTATION OF THE GREEN FUNCTION AND ITS DERIVATIVES FOR FLOATING OR SUBMERGED BODIES IN DEEP WATER

Chunmei Xie*
LHEEA
Ecole Centrale de Nantes
Nantes, 44300, France
Email: chunmei.xie@ec-nantes.fr

Aurélien Babarit
François Rongère
Alain H. Clément

LHEEA
Ecole Centrale de Nantes
Nantes, 44300, France

ABSTRACT

A new acceleration technique for the computation of first order hydrodynamic coefficients for floating bodies in frequency domain and in deep water is proposed. It is based on the classical boundary element method (BEM) which requires solving a boundary integral equation for distributions of sources and/or dipoles and evaluating integrals of Kelvin's Green function and its derivatives over panels. The Kelvin's Green function includes two Rankine sources and a wave term. In present study, for the two Rankine sources, analytical integrations of strongly singular kernels are adopted for the linear density distributions. It is shown that these analytical integrations are more accurate and faster than numerical integrations. The wave term is obtained by solving Clément's ordinary differential equations (ODEs) [1] and an adaptive numerical quadrature is performed for integrations over the panels. It is shown here that the computational time of the wave term by solving the ODEs is greatly reduced compared to the classical integration method [7].

INTRODUCTION

Boundary Element Methods (BEM)s are popular in the academia and the industry for solving three-dimensional wave radiation and diffraction problems with one or multi floating or submerged bodies. In the BEMs, the initial three-dimensional problem for the velocity potential is replaced by a two-dimensional problem on the fluid domain's boundary surfaces.

Among the various BEM approaches, the constant panel method (CPM) was proposed for unbounded fluid configurations by Hess and Smith [2]. The surfaces of the bodies are discretised in flat triangles or quadrilaterals. The sources or sinks are distributed over the panels with a constant density for each panel. However, there is a jump in the potential between two adjacent panels in such zeroth order CPM. Higher order panel representations are expected to be more accurate than the CPM for the same discretization level [3]. In the present paper, a linear panel method (LPM), or first order panel method, has been adopted. The body geometry is discretised with flat triangles. A collocation method with the unknowns located on the vertices of the triangles is implemented. LPM is a first order method with less computational burden compared to higher order methods and more accurate compared to constant method.
Further, an important part of the numerical burden in the case of forced oscillations and wave-induced motions of bodies is the computation of free surface Green function. Fortunately, for linearised potential flow in the frequency domain and in deep wa-

*Address all correspondence to this author.

ter, exact formulations of the Green function satisfying both the Laplace equation and the linearised free surface condition are available. In 1960, Wehausen and Laitone [4] reviewed preliminary developments and provided the classical expression of the Green function and several alternative integral representations. Two years later, Ursell [5] used a spherical harmonics expansion to get the Green function for a heaving hemisphere. Great improvements for the computation of the Green function in three dimensions have been achieved in the 1980s. Two complementary near-field and far-field representations in terms of the exponential integral have been defined where an asymptotic expansion and a convergent ascending-series expansion for the Green function have been tested by Noblesse [6]. In 1985, Newman [7] provided a new algorithm for computing the free surface Green function and its derivatives in infinite and constant finite depth. He defined regions of the parameters space with proper polynomial expansions in every region. Peter and Meylan [8] proposed an eigenfunction expansion representation for the free surface Green function which is easy to evaluate numerically. In 2011, a semi-analytical method was used with Haskind-Havelock kernel calculated by a singularity substractive technique [9]. The multipole expansion of the free surface Green's function and its derivative has been extended in a 3D fast multipole algorithm [10].

It can be noticed that all the algorithms mentioned above are based on evaluating an integral. In 1998, fourth order ODEs were introduced by Clément for the time-domain free surface Green function and its derivatives [15]. Much later [1], he transposed those fourth order time domain ODE into second order ODE for the free surface Green function in the frequency domain. For the time-domain Green function, a semi-analytical precise integration method [11] and a analytical method based on Taylor series expansion [12] have been developed replacing the standard four-step Runge-Kutta method (RK4) to solve the fourth order ODEs. Recently, still in time-domain, Bingham [13] compared the efficiency of three ODE-based methods and the standard algorithms developed by Newman [14]. He found the standard algorithm based on asymptotic expansions and polynomial interpolation is more efficient than any of the existing ODE-based methods. Using a numerical method to solve the ODE may be more practical and faster than evaluating integrals in frequency domain. The aim of the present paper is precisely to evaluate the benefit one may achieve from using the frequency-domain ODEs to compute the Green function and its derivatives in comparison to the classical approach.

PROBLEM DESCRIPTION

The first order wave radiation problem in frequency domain and in infinite water depth is considered. It is assumed that the fluid is inviscid, incompressible and the flow irrotational. The time factor of the complex potential is taken as $e^{-i\omega t}$ with ω the wave frequency. The total radiation potential can be decomposed as $\phi_R = \sum_j V_{Ej}\phi_j$ with $j = 1,2,...,6$ where V_{Ej} denotes the amplitude of the generalized body velocity. The BVP equations are shown in Eqn. 1.

$$\begin{cases} \Delta\phi_j(M) = 0 & M \in \Omega \\ \frac{\partial\phi_j(M)}{\partial n_B} = \vec{n}_j\,|_M & M \in S_B \\ \frac{\partial\phi_j(M)}{\partial z} = \frac{\omega^2}{g}\phi_j(M) & M \in S_F \\ \phi_j(M) \to 0 & M \to \infty \end{cases} \tag{1}$$

where $\vec{n}_B$ is the generalised normal vector on the body surface, g is the gravity, n_j is the generalized normal and z is the vertical axis. Fig. 1 shows the illustration of the problem and the basic notation in this paper. It should be noted that, the body can be submerged or floating and that there can be single or multi-bodies with any geometry.

With use of Green's identities, a Fredholm equation of the second kind over the body surface S_B can be derived.

$$\Omega\mu(M) - \frac{1}{4\pi}\iint_{S_B}\mu(P)\frac{\partial}{\partial n_P}G_\infty(M,P)dS(P) = \frac{1}{4\pi}\iint_{S_B}\vec{V_E}\cdot\vec{n}\,|_P\,G_\infty(M,P)dS(P) \tag{2}$$

P and M are the source and field points, respectively. A mixed distribution of sources and normal dipoles is used with $\sigma(P) = (\frac{\partial\phi}{\partial n})_P = \vec{V_E}\cdot\vec{n}\,|_P$ and $\mu(P) = -\phi(P)$. σ and μ are densities of sources and normal dipoles over the body surface, G_∞ is the Kelvin's Green function in deep water. For the first term in Eqn. 2, we have $\Omega = 1 - \frac{\widetilde{\Omega}(M)}{4\pi}$, where $\widetilde{\Omega}(M)$ is the solid angle in the body. The solid angle can be calculated after the discretization of Eqn. 2 considering $\mu = 1$ and $\sigma = 0$.

Eventually, the added mass (A_{ij}) and radiation damping coefficients (B_{ij}) are defined in Eqn. 3 with $i, j = 1,2,...,6$.

$$\begin{aligned} A_{ij} &= \rho\iint_{S_B}\mathbf{Re}(\phi_j)n_i ds \\ B_{ij} &= \rho\omega\iint_{S_B}\mathbf{Im}(\phi_j)n_i ds \end{aligned} \tag{3}$$

ODES FOR THE GREEN FUNCTION

The Kelvin's Green function includes two Rankine sources and a wave term $G_\infty = \frac{1}{MP} - \frac{1}{MP'} + G$ with P' the image point of P with respect to the free surface $z = 0$. In the present study, the analytical integrations of strongly singular kernels of the two Rankine sources are used for the linear density distribution. The detailled derivation of these coefficients can be found in Appendix A.

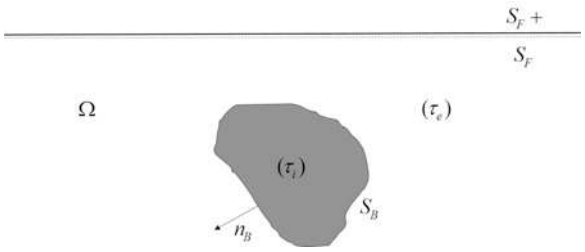

FIGURE 1. ILLUSTRATION

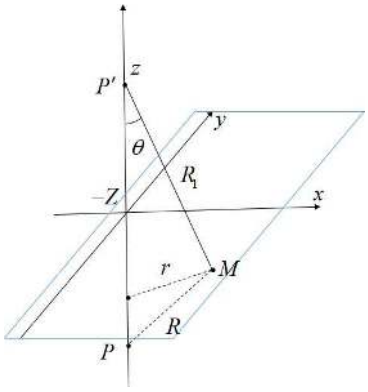

FIGURE 2. THE SOURCE AND FIELD POINTS

Let us consider a field point $M(x_M, y_M, z_M)$ and a source point $P(x_P, y_P, z_P)$ with $z_M \leqslant 0, z_P \leqslant 0$. r is the relative horizontal distance between M and P, $Z = z_M + z_P$ and $-Z$ is the vertical distance between the field point M and the image of the source point relative to the free surface P' as seen in Fig. 2. The Kelvin's Green function in the frequency domain and in water of infinite depth is [4]:

$$\begin{aligned} &G_\infty(r,Z,i\omega) = G_0(M,P) + G(r,Z,i\omega) \\ &= \frac{1}{R} - \frac{1}{R_1} + 2PV\int_0^\infty \frac{k}{k-k_0} e^{kZ} J_0(kr)dk - 2i\pi sgn(\omega) k_0 e^{k_0 Z} J_0(k_0 r) \end{aligned} \tag{4}$$

with R the distance between the source point M and the field point P, and R_1 the distance between the image source point P' and the field point M. $k_0 = \omega^2/g$, and $PV\int$ means the Cauchy's principal value of the integral. In 2013, Clément [1] derived a second order ODE for $G(r,Z,i\omega)$ based on non-dimensional variables. In this section, this ODE is studied and two similar ODEs for the gradient of the Kelvin Green function are given.

Nondimensionalization

Let us clarify the nondimensionalization of the Green function $G(r,Z,i\omega)$ which satisfies the ODE. Let: $\widetilde{R} = R/L$, $\widetilde{R}_1 = R_1/L$, $\widetilde{r} = r/L$, $\widetilde{Z} = Z/L$, $\widetilde{k}_0 = k_0 L = \omega^2 L/g = \widetilde{\omega}^2$, $\widetilde{k} = kL$, where L denotes a reference length.

$$\begin{aligned} &LG_\infty(r,Z,i\omega) = LG_0(M,P) + LG(r,Z,i\omega) \\ &= \frac{1}{\widetilde{R}} - \frac{1}{\widetilde{R}_1} + 2PV\int_0^\infty \frac{\widetilde{k}}{\widetilde{k}-\widetilde{k}_0} e^{\widetilde{k}\widetilde{Z}} J_0(\widetilde{k}\widetilde{r})d\widetilde{k} - 2i\pi sgn(\omega)\widetilde{k}_0 e^{\widetilde{k}_0\widetilde{Z}} J_0(\widetilde{k}_0\widetilde{r}) \end{aligned} \tag{5}$$

Eqn. 11 of Clément's paper is the ODE for $\widetilde{G}(r,Z,i\omega) = LG(r,Z,i\omega)$ with $\widetilde{k}_0 = \widetilde{\omega}^2$. For sake of simplicity, $\sim$ will be omitted hereafter. Thus:

$$G(r,Z,i\omega) = 2PV\int_0^\infty \frac{k}{k-k_0} e^{kZ} J_0(kr)dk - 2i\pi sgn(\omega) k_0 e^{k_0 Z} J_0(k_0 r) \tag{6}$$

with $k_0 = \omega^2$ and $G(r,Z,i\omega)$ satisfies the second order ODE below:

$$\frac{\omega^2}{4} G_{\omega\omega} - \omega(\omega^2 Z + \frac{3}{4}) G_\omega + (\omega^4(r^2+Z^2) + \omega^2 Z + 1)G = \frac{2(1+Z\omega^2)}{\sqrt{r^2+Z^2}} \tag{7}$$

In this paper, the derivative with respect to the subscripting variable is intended.

ODEs For The Derivatives Of The Green Function

From Eqn 2, the gradient of the Green function is needed to implement the BEM. From the linear distribution rule in Appendix A Eqn. 19, we have

$$\begin{aligned} I_\mu &= \iint_{S_i} \mu(P) \frac{\partial}{\partial n_P} G ds(P) \\ &= \iint_{S_i} (\mu(C) + \vec{\nabla}_S \mu \cdot \overrightarrow{CP}) \vec{n}_p \cdot \vec{\nabla} G dS(P) \end{aligned} \tag{8}$$

With

$$\begin{aligned} \vec{\nabla} G &= \frac{\partial G}{\partial x_p}\vec{x} + \frac{\partial G}{\partial y_p}\vec{y} + \frac{\partial G}{\partial z_p}\vec{z} \\ &= \frac{\partial G}{\partial r}\frac{x_p - x_m}{r}\vec{x} + \frac{\partial G}{\partial r}\frac{y_p - y_m}{r}\vec{y} + \frac{\partial G}{\partial Z}\vec{z} \end{aligned} \tag{9}$$

From the equations above, only G_r and G_Z are needed to get the gradient of G. By differentiating Eqn. 6 with respect to r and Z, one can show:

$$G_r(r,Z,i\omega) = -2PV\int_0^\infty \frac{k^2}{k-k_0} e^{kZ} J_1(kr)dk + 2i\pi sgn(\omega) {k_0}^2 e^{k_0 Z} J_1(k_0 r) \tag{10}$$

$$G_Z(r,Z,i\omega) = 2PV\int_0^\infty \frac{k^2}{k-k_0} e^{kZ} J_0(kr)dk - 2i\pi sgn(\omega) {k_0}^2 e^{k_0 Z} J_0(k_0 r) \tag{11}$$

The ODEs for the derivatives of the Green function in direction r and Z in the time domain can be found in Clément's paper [15]. By introducing the auxiliary function $S(r,Z;t) = \mathbb{H}(t) * F(r,Z;t)$

with $\mathbb{H}$ the Heaviside step function, by taking into account the differential relation between the Heaviside and the Dirac distribution and using the same convention and notation for the Fourier transform as Clément - and Shen et al [16]- one can derive the two ODEs for the derivatives of G with respect to r and Z namely:

$$\frac{\omega^2}{4}G_{r\omega\omega}-\omega(\omega^2 Z+\frac{7}{4})G_{r\omega}+(\omega^4(r^2+Z^2)+3\omega^2 Z+3)G_r=\frac{-6r(1+Z\omega^2)}{(r^2+Z^2)^{3/2}} \tag{12}$$

$$\begin{aligned}&\frac{\omega^2}{4}G_{Z\omega\omega}-\omega(\omega^2 Z+\frac{7}{4})G_{Z\omega}+(\omega^4(r^2+Z^2)+3\omega^2 Z+4)G_Z\\&=\frac{-4Z(2+Z\omega^2)+2r^2\omega^2}{(r^2+Z^2)^{3/2}}\end{aligned} \tag{13}$$

ODEs Analysis

Equations 7,12,13 are three ODEs for G, G_r, G_Z with respect to frequency ω, respectively. They have similar properties. For these second-order ODEs, $\omega=0$ is a regular singular point or called nonessential singularity, where the growth of solution is bounded in any small sector by an algebraic function [17]. These ODEs whose solutions are the Green function and its derivatives are similar to Bessel differential equation whose solutions are Bessel functions or the Hypergeometric equation whose solution is the hypergeometric function. The imaginary parts of G, G_r, G_Z (see Eqns. 6, 10, 11) are expressed analytically and are easy and fast to calculate by using standard libraries. It is easy to check that they are solutions of the homogenous ODEs 7,12,13. The most challenging part in solving a radiation problem with Kelvin's Green function and its derivatives is the computation of their real parts.

When $\omega=0$, we have the real part of G, G_r, G_Z as in the following:

$$\begin{aligned}\mathbf{Re}(G(r,Z,0))&=\frac{2}{\sqrt{r^2+Z^2}},\mathbf{Re}(G_\omega(r,Z,0))=0\\\mathbf{Re}(G_r(r,Z,0))&=\frac{-2r}{\sqrt{r^2+Z^2}^3},\mathbf{Re}(G_{r\omega}(r,Z,0))=0\\\mathbf{Re}(G_Z(r,Z,0))&=\frac{-2Z}{\sqrt{r^2+Z^2}^3},\mathbf{Re}(G_{Z\omega}(r,Z,0))=0\end{aligned} \tag{14}$$

For these ODEs, $\omega=0$ is a regular singular point; this may results in failures of numerical ODE integrators at this very initial condition. A simple alternative is to shift the initial conditions to a small positive initial value ω_0 of the frequency variable where the fonction and its derivatives can be initialized at this unique starting value by classical Green function routines.

As ω_0 tends to 0, one can see that the first order coefficients, zero order coefficients and the right hand sides of equations 7, 12, 13 become very large. If the initial conditions for G, G_ω, $G_r, G_{r\omega}$ and $G_Z, G_{Z\omega}$ are not accurate enough or if the frequency step is not small enough, the errors of the first terms, second terms and the right hand sides grow very fast and the numerical results have been found to diverge. For practical applications in seakeeping BEM computer codes, ω_0 will be chosen as the lower bound of the user defined frequency range of interest, which is larger than zero as the purely zero frequency case has no physical meaning in this context. In this paper, $\omega_0=1$ has been chosen. It is the same ω_0 as in Shen et al's study [16].

The ODEs In 'Natural Variables'

The initial variables (r,Z,ω) in Eqn. 7, 12, 13 can be replaced by $\mu=-\frac{Z}{R_1}$, $\varpi=\omega\sqrt{R_1}$ similar as in Clément's paper for the ODEs in the time domain [15]. From the definition of μ, $\mu=\cos(\theta)\in[0,1]$ (see Fig. 2). Let us define $\tilde{G}=\frac{R_1}{2}G$, $\tilde{G}_r=\frac{R1^2}{2}G_r$, $\tilde{G}_Z=\frac{R1^2}{2}G_Z$. One obtains three ODEs which only depend on the variables μ and ϖ for these functions. The μ and ϖ are called 'natural variables' herein without further justification. After this substitution, the ODEs for the Green function and its derivatives with three variables have been transformed into ODEs in the two 'natural variables':

$$\begin{aligned}&\frac{1}{4}\varpi^2\tilde{G}_{\varpi\varpi}+(\mu\varpi^3-\frac{3}{4}\varpi)\tilde{G}_\varpi+(\varpi^4-\mu\varpi^2+1)\tilde{G}=1-\varpi^2\mu\\&\frac{1}{4}\varpi^2\tilde{G}_{r\varpi\varpi}+(\mu\varpi^3-\frac{7}{4}\varpi)\tilde{G}_{r\varpi}+(\varpi^4-3\mu\varpi^2+3)\tilde{G}_r=-3\sqrt{1-\mu^2}(1-\mu\varpi^2)\\&\frac{1}{4}\varpi^2\tilde{G}_{Z\varpi\varpi}+(\mu\varpi^3-\frac{7}{4}\varpi)\tilde{G}_{Z\varpi}+(\varpi^4-3\mu\varpi^2+4)\tilde{G}_Z=\\&2\mu(2-\varpi^2\mu)+(1-\mu^2)\varpi^2\end{aligned} \tag{15}$$

VALIDATIONS

Added mass coefficient for a floating hemisphere at zero and infinite frequency

Let us consider a floating hemisphere as a benchmark test case. In Hulme [18], the added mass coefficient of a heaving hemisphere for zero frequency and infinite frequency are given as 0.8310 and 0.5, respectively. For these asymptotic values, there is no wave term and therefore the damping coefficients are zero. Thus, the Green function for zero frequency and infinite frequency is reduced to:

$$\begin{aligned}G_\infty(r,Z,0)&=\frac{1}{R}+\frac{1}{R_1}\\G_\infty(r,Z,\infty)&=\frac{1}{R}-\frac{1}{R_1}\end{aligned} \tag{16}$$

We discretised Eqn. 2 with flat triangular panels. The integration of two Rankine sources are calculated by analytical expressions

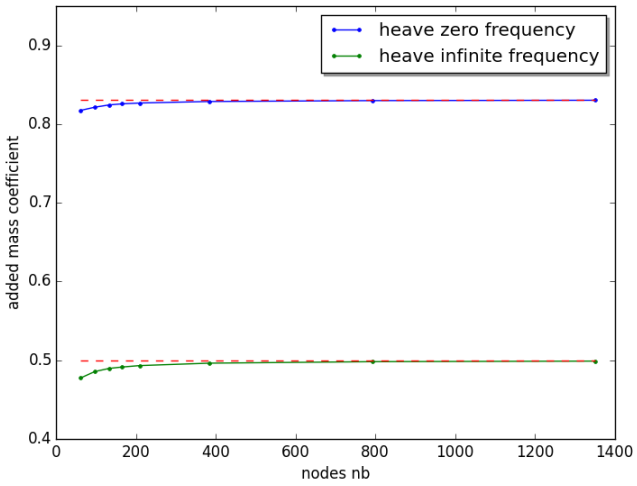

FIGURE 3. MESH CONVERGENCE STUDY FOR THE ADDED MASS COEFFICIENT OF A HEAVING HEMISPHERE AT ZERO AND INFINITE FREQUENCIES

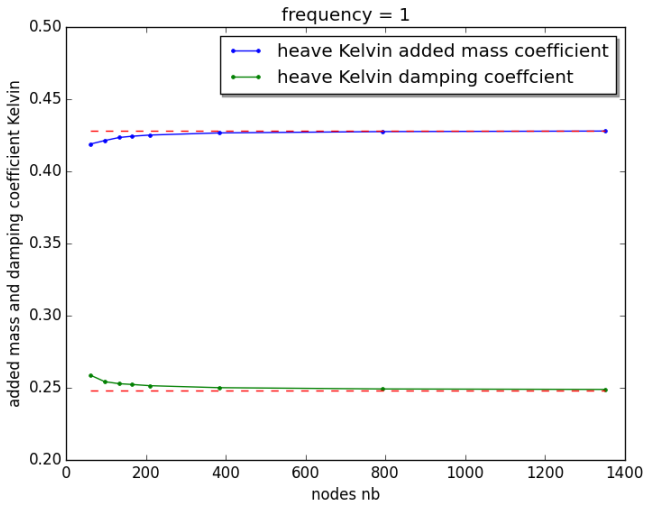

FIGURE 4. THE ADDED MASS COEFFICIENT AND DAMPING COEFFICIENT OF A HEAVING HEMISPHERE WITH FREQUENCY UNIT CONVERGENCE WITH MESH REFINEMENT

which can be found in Appendix A. The discretization leads to a linear matrix problem for the velocity potential. and the linear system is solved by the LAPACK routine_gesv. The added mass and damping coefficients are calculated as the definitions shown in Eqn. 3. Results for eight meshes more and more refined are given with 62, 97, 133, 165, 210, 383, 792 and 1351 nodes. The radius of the hemisphere is $R = 1$. The results for the added mass coefficient at zero frequency and infinite frequency are shown in Fig. 3. The blue line is the numerical result for zero frequency and the green one is for infinite frequency. The red dashed lines are the values in Hulme's paper. A good agreement of the added mass is found. The analytical integrations of the Rankine source $1/R_1$ with image of source point and the field point is validated by this agreements.

For testing the wave term and the Gauss quadrature, a heaving hemisphere oscillating with frequency 1 is tested for the same meshes as mentioned above.

The same code structure as for the calculations of the added mass at zero and infinite frequencies. The difference is in the calculation of the frequency dependent influence coefficients in which the wave part of the Green function is added. Surface integrals of the following form must be evaluated:

$$\begin{aligned} S_F(M) &= \iint_{S_i} G(P,M)\vec{V}_E \cdot \vec{n}|_P dS(P) \\ D_F(M) &= \iint_{S_i} \frac{\partial}{\partial n} G(P,M)\mu(P) dS(P) \end{aligned} \tag{17}$$

We recall that $\vec{V}_E \cdot \vec{n}|_P$ and $\mu(P)$ following the linear distributions rule in Appendix A Eqn. 19 and we chose the fifth order of Gaussian quadrature formulas. The details of Gaussian quadrature for triangles can be found in Deng's note [19]. Here, the wave term of Kelvin's Green function was calculated by Newman's algorithm [7].

For $\omega = 1$, $R = 1$, the added mass coefficient and damping coefficient are 0.4284 0.2484, respectively. As shown in Fig. 4, the blue line and green line are added mass coefficients and damping coefficients. The red dashed lines are the values given by Hulme. One can see that the code converges quickly towards the analytical values of the literature. It shows that the Kelvin's Green function and linear boundary element method are correctly implemented.

Speed-Up Of Computation Of Green Function And Its Derivatives By Using ODEs

As discussed above, the computation of the real parts of the Green function and its derivatives is expected to be time-consuming due to the direct evaluation of the integral in the Green function. In this section, the second order ODEs are used and the computational time is compared to the one for the integral evaluation approach. For this later approach, the implementation of Newman's algorithm by Choi [19] was used here. He used FORTRAN-90. His implementation has been used in the in-house code "SOSMAT" of Pusan national university. Note that his code is also used for initialisation of the ODEs.

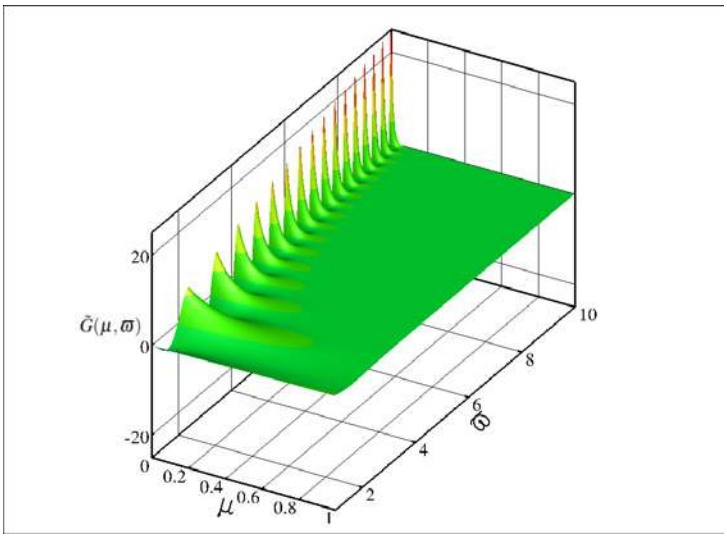

FIGURE 5. THE GREEN FUNCTION WITH NATURAL VARIABLES $\tilde{G}(\mu,\varpi)$

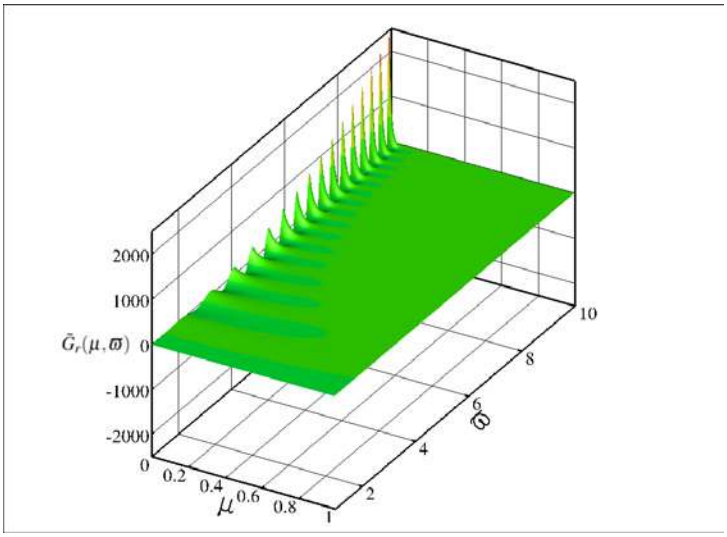

FIGURE 6. THE DERIVATIVE OF GREEN FUNCTION IN DIRECTION r WITH NATURAL VARIABLES $\tilde{G}_r(\mu,\varpi)$

For the comparisons, M as the field point is located at the vertices of the triangles and P as the source point is located on the triangles. $\mu \in [0,1[$. $\Delta\mu = 0.099$, $\varpi \in [1,10]$ and $\Delta\varpi = 0.001$ were used. The classical numerical integrator RK4 was adopted here.

The Green function and its derivatives with respect to r and Z in natural variables can been seen in Fig. 5, 6, 7. An absolute error or relative accuracy of 6 decimals has been selected for

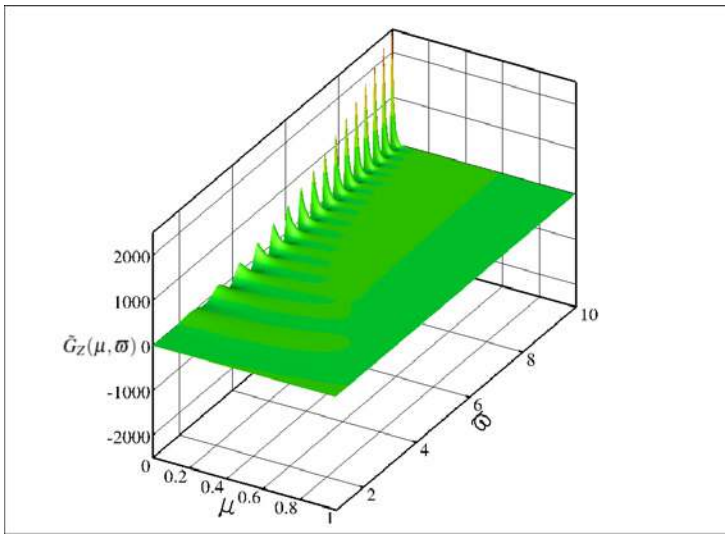

FIGURE 7. THE DERIVATIVE OF GREEN FUNCTION IN DIRECTION Z WITH NATURAL VARIABLES $\tilde{G}_Z(\mu,\varpi)$

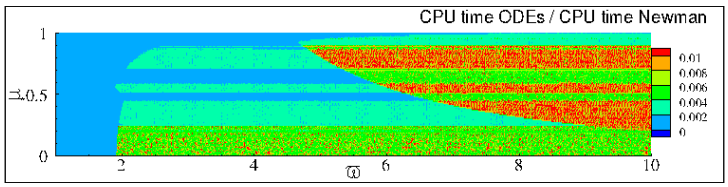

FIGURE 8. THE CPU TIME RATIO OF ODES AND NEWMAN'S ALGORITHM

all approximations of the Green function and its derivatives for the initial value of ODEs and comparison values of Newman's algorithm.

The CPU time to obtain the dataset in Fig. 5, 6 and 7 was 0.016s for the ODEs whereas it was 3.648s for Newman's algorithm leading to a mean global ratio CPU(ODE)/CPU(Newman) of 227. The mean CPU time for the computation of the Green function and its derivatives with one single set of (r,Z,ω) by the ODEs and the Newman's algorithm are $1.78 * 10^{-9}$s and $4.05 * 10^{-6}$s, respectively. The local CPU time ratio of the ODEs and the Newman algorithm is plotted in Fig. 8. For each μ, the CPU time for ODEs for each frequency is the average value of CPU time of all $\varpi \in [1,10]$; the maximum value of this ratio is shown to be around 0.01 (red scale). From those results, it appears that the ODEs' approach is very efficient. It can greatly reduce the computational time of calculating the Green function and its derivatives in such seakeeping BEM solvers. Note that the calculations were performed on a PC with Intel(R) Core(TM) i7-6700 CPU @ 3.40GHz.

CONCLUSION

A method to calculate the first order hydrodynamic coefficients for floating or submerged bodies in deep water and in frequency domain is presented. Based on the classical boundary element method, it requires solving a boundary integral equations for linear mixed distributions of sources and normal dipoles and necessitate evaluation of integrals of Kelvin's Green function. Flat triangles are used to approximate the body surface and the integral equation is replaced by a set of linear algebraic equations. Two Rankine sources and a wave term are included in Kelvin's Green function. The integrals of linear density for the two Rankine sources are calculated by analytical expressions. The wave term is obtained by integrating Clément's ODEs with a numerical integrator RK4, and this is shown significantly reduce the computational time compared to integral evaluation. For the Green function and its derivatives in 'natural variables', the computational time of integral evaluation is found by classical routines to be about 200 times greater compared to the ODEs.

ACKNOWLEDGMENT

The authors gratefully acknowledge financial support from China Scholarship Council. The first author thanks Mr. Y.M. Choi for his help.

References

[1] Clément, A., 2013. "A second order ordinary differential equation for the frequency domain green function". In 28th International Workshop on Water Waves and Floating Bodies.

[2] Hess, J. L., and Smith, A., 1962. Calculation of non-lifting potential flow about arbitrary three-dimensional bodies. Tech. rep., Douglas Aircraft Co Long Beach CA.

[3] Teng, B., and Taylor, R. E., 1995. "New higher-order boundary element methods for wave diffraction/radiation". *Applied Ocean Research,* ***17***(2), pp. 71–77.

[4] Wehausen, J., and Laitone, E., 1960. *Surface Waves*. Springer.

[5] Ursell, F., 1962. The periodic heaving motion of a half-immersed sphere: The analytic form of the velocity potential long-wave asymptotics of the virtual-mass coefficient. Tech. rep., VICTORIA UNIV OF MANCHESTER (UNITED KINGDOM).

[6] Noblesse, F., 1982. "The green function in the theory of radiation and diffraction of regular water waves by a body". *Journal of Engineering Mathematics,* ***16***(2), pp. 137–169.

[7] Newman, J., 1985. "Algorithms for the free-surface green function". *Journal of engineering mathematics,* ***19***(1), pp. 57–67.

[8] Peter, M. A., and Meylan, M. H., 2004. "The eigenfunction expansion of the infinite depth free surface green function in three dimensions". *Wave Motion,* ***40***(1), pp. 1–11.

[9] D'elía, J., Battaglia, L., and Storti, M., 2011. "A semi-analytical computation of the kelvin kernel for potential flows with a free surface". *Computational & Applied Mathematics,* ***30***(2), pp. 267–287.

[10] Borgarino, B., Babarit, A., Ferrant, P., et al., 2011. "Extension of free-surface green's function multipole expansion for infinite water depth case". *International Journal of Offshore and Polar Engineering,* ***21***(03).

[11] Chuang, J., Qiu, W., and Peng, H., 2007. "On the evaluation of time-domain green function". *Ocean engineering,* ***34***(7), pp. 962–969.

[12] Li, Z.-F., Ren, H.-L., Tong, X.-W., and Li, H., 2015. "A precise computation method of transient free surface green function". *Ocean Engineering,* ***105***, pp. 318–326.

[13] Bingham, H. B., 2016. "A note on the relative efficiency of methods for computing the transient free-surface green function". *Ocean Engineering,* ***120***, pp. 15–20.

[14] Newman, J., 1992. "The approximation of free-surface green functions". In *Wave asymptotics*, Vol. 107. Cambridge University Press Cambridge, UK.

[15] Clement, A., 1998. "An ordinary differential equation for the green function of time-domain free-surface hydrodynamics". *Journal of Engineering mathematics,* ***33***(2), pp. 201–217.

[16] Shen, Y., Yu, D., Duan, W., and Ling, H., 2016. "Ordinary differential equation algorithms for a frequency-domain water wave green's function". *Journal of Engineering Mathematics,* ***100***(1), pp. 53–66.

[17] Bender, C. M., and Orszag, S. A., 2013. *Advanced mathematical methods for scientists and engineers I: Asymptotic methods and perturbation theory*. Springer Science & Business Media.

[18] Hulme, A., 1982. "The wave forces acting on a floating hemisphere undergoing forced periodic oscillations". *Journal of Fluid Mechanics,* ***121***, pp. 443–463.

[19] Deng, S. Quadrature formulas in two dimensions. Math 5172 - Finite Element Method.

[20] John, L., 1964. "Calculation of non-lifting potential flow about arbitrary three dimensional bodies". *Journal of Ship Research,* ***8***, pp. 22–44.

[21] Guevel, P., 1976. *Corps solide animé d'un mouvement quelconque dans un fluide illimité*. ENSM.

[22] Letournel, L., 2015. "Développement d'un outil de simulation numérique basé sur l'approche" weak-scatterer" pour l'étude des systèmes houlomoteurs en grands mouvements". PhD thesis, Ecole Centrale de Nantes.

Appendix A: Analytical Integrations for Linear Distributions Over a Triangle

The analytical integrations of strongly singular kernels of the two Rankine sources are used for the linear density distribution. The analytical integrations of constant sources density is classical and can be found in John's paper [20]. In 1976, Guevel [21] gave analytical formulas for the integration of mixed of constant sources and dipoles distributions. Recently, Letournel [22] extended the analytical expressions to linear sources and normal dipoles distributions. In this section, the results of those analytical integrations of linear sources and linear normal dipoles by Letournel are recalled, with corrections. The integrations with the image point P' are given.

Plane triangle surface elements are used to discretize the body surface. The integration for linear distributions of sources over one triangle is shown to be.

$$\begin{aligned} I_\sigma(M) &= \iint_{S_i} \sigma(P)\frac{1}{MP}dS(P) \\ &= (\sigma(C)+\vec{\nabla}_S\sigma\cdot\overrightarrow{CM})\iint_{S_i}\frac{1}{MP}dS(P)+\vec{\nabla}_S\sigma\cdot\iint_{S_i}\frac{\overrightarrow{MP}}{MP}dS(P) \\ &= (\sigma(C)+\vec{\nabla}_S\sigma\cdot\overrightarrow{CM})\iint_{S_i}\frac{1}{MP}dS(P)-\vec{\nabla}_S\sigma\cdot\oint_{C_i}MP\vec{n}\wedge\overrightarrow{dl} \\ &= \sigma(M)S_\sigma(M)-\vec{\nabla}_S\sigma(M)\cdot\vec{I}_\sigma(M) \end{aligned} \tag{18}$$

with $S_\sigma(M)=\iint_{S_i}\frac{1}{MP}dS(P)$, $\vec{I}_\sigma(M)=\oint_{C_i}MP\vec{n}\wedge\overrightarrow{dl}$. $\vec{\nabla}_S$ is the surface gradient using the same parametrization as in Letournel [22] . For any linear distribution f, we have,

$$f(P)=f(C)+\vec{\nabla}_S f\cdot\overrightarrow{CP} \tag{19}$$

where C is the center of triangle, $\vec{n}$ is normal vector of the triangle pointing towards the fluid. The sign of $\vec{I}_\sigma(M)$ is corrected compared to Letournel's paper.

The integration for the linear distribution of normal dipoles over one triangle is shown to be:

$$\begin{aligned} I_\mu(M) &= \iint_{S_i}\mu(P)\frac{\partial}{\partial n_P}\frac{1}{MP}dS(P) \\ &= (\mu(C)+\vec{\nabla}_S\mu\cdot\overrightarrow{CM})\iint_{S_i}\frac{\partial}{\partial n_P}\frac{1}{MP}dS(P)+\iint_{S_i}\frac{\partial}{\partial n_P}\frac{1}{MP}(\vec{\nabla}_S\mu\cdot\overrightarrow{MP})dS(P) \\ &= (\mu(C)+\vec{\nabla}_S\mu\cdot\overrightarrow{CM})\iint_{S_i}\frac{\partial}{\partial n_P}\frac{1}{MP}dS(P)-\vec{\nabla}_S\mu\cdot\oint_{C_i}\frac{\overrightarrow{MP}}{MP}\wedge\overrightarrow{dl} \\ &= \mu(M)S_\mu(M)-\vec{\nabla}_S\mu\cdot\vec{I}_\mu(M) \end{aligned} \tag{20}$$

with $S_\mu(M)=\iint_{S_i}\frac{\partial}{\partial n_P}\frac{1}{MP}dS$, $\vec{I}_\mu(M)=\oint_{C_i}\frac{\overrightarrow{MP}}{MP}\wedge\overrightarrow{dl}$.

In the following, analytical expressions are recalled for the four integrals above: surface integral of source S_σ, line integral of source $\vec{I}_\sigma$, surface integral of dipole S_μ and line integral of source $\vec{I}_\mu$. The collocation method is considered, thus the field point M can be located at the vertices of the triangles or at some other point except the triangle surface. For $I'_\sigma(M)=\iint_{S_i}\sigma(P)\frac{1}{MP'}dS(P)$ and $I'_\mu(M)=\iint_{S_i}\mu(P)\frac{\partial}{\partial n_P}\frac{1}{MP'}ds(P)$ where the P' is the image point of P with respect to the horizontal plane $z=0$.

$$\begin{aligned} I'_\sigma(M) &= \iint_{S_i}\sigma(P)\frac{1}{MP'}dS(P) \\ &= (\sigma(C)+\vec{\nabla}_S\sigma\cdot\overrightarrow{CM})\iint_{S_i}\frac{1}{MP'}dS(P)+\vec{\nabla}_S\sigma\cdot\iint_{S_i}\frac{\overrightarrow{MP}}{MP'}dS(P) \\ &= (\sigma(C)+\vec{\nabla}_S\sigma\cdot\overrightarrow{CM})\iint_{S_i}\frac{1}{MP'}dS(P) \\ &+\vec{\nabla}_S\sigma\cdot(\iint\frac{\overrightarrow{MP'}}{MP'}dS(P)-2\iint\frac{\overrightarrow{z_{P'}}-\overrightarrow{z_M}}{MP'}dS(P)-2\iint\frac{\overrightarrow{z_M}}{MP'}dS(P)) \end{aligned} \tag{21}$$

$$\begin{aligned} I'_\mu(M) &= \iint\mu(P)\frac{\partial}{\partial n_p}\frac{1}{MP'}dS(P) \\ &= (\mu(C)+\overrightarrow{\nabla_S}\mu\cdot\overrightarrow{CM})\iint\frac{\partial}{\partial n_p}\frac{1}{MP'}dS(P) \\ &+\overrightarrow{\nabla_S}\mu\cdot(\iint\overrightarrow{MP'}\frac{\partial}{\partial n_p}\frac{1}{MP'}dS(P)-2\iint(\overrightarrow{z_{P'}}-\overrightarrow{z_M})\frac{\partial}{\partial n_p}\frac{1}{MP'}dS(P)- \\ &2\iint\overrightarrow{z_M}\frac{\partial}{\partial n_p}\frac{1}{MP'}dS(P)) \end{aligned} \tag{22}$$

Where $\overrightarrow{z_{P'}}=z_{P'}*\vec{k}_z$, $\overrightarrow{z_M}=z_M*\vec{k}_z$, and $(\vec{k}_x,\vec{k}_y,\vec{k}_z)$ is the global unit coordinates of this problem with the field point $M(x_M,y_M,z_M)$ and the image of the source point $P'(x'_P,y'_P,z'_P)$. Analytical expressions of $S'_\sigma(M)=\iint_{S_i}\frac{1}{MP'}dS(P)$, $\vec{I}'_\sigma(M)=-\vec{\nabla}_S\sigma\cdot\iint_{S_i}\frac{\overrightarrow{MP'}}{MP'}dS(P)=\oint_{C_i}MP'\vec{n}\wedge\overrightarrow{dl}$, $S'_\mu(M)=\iint_{S_i}\frac{\partial}{\partial n_P}\frac{1}{MP'}dS$, $\vec{I}'_\mu(M)=-\iint_{S_i}\frac{\partial}{\partial n_P}\frac{1}{MP'}(\vec{\nabla}_S\mu\cdot\overrightarrow{MP'})dS(P)=\oint_{C_i}\frac{\overrightarrow{MP'}}{MP'}\wedge\overrightarrow{dl}$ can be obtained by mirroring the expression of the four integrals above. It should be noted that the order of vertices must be reverted.

Surface integral of term $S_\sigma(M)$

- For $M\notin S_i$, the integral $S_\sigma(M)=\iint_{S_i}\frac{1}{MP}dS(P)$ has an analytical solution given by Guevel [21].

$$S_\sigma(M)=\sum_{k=1}^{3}\frac{N_k^t}{2d_k}\log(\frac{N_k^1}{D_k^1})-2|Z|\arctan(\frac{N_k^t}{D_k^t}) \tag{23}$$

with

$$\begin{cases} R_k=\|\overrightarrow{P_kM}\| \\ d_k=\|\overrightarrow{P_kP_{k+1}}\| \\ Z=\overrightarrow{GM}\cdot\vec{n} \\ N_k^1=R_{k+1}+R_k+d_k \\ D_k^1=R_{k+1}+R_k-d_k \\ N_k^t=2\overrightarrow{P_kM}\cdot(\vec{n}\wedge\overrightarrow{P_kP_{k+1}}) \\ D_k^t=(R_{k+1}+R_k)^2-d_k^2+2|Z|(R_{k+1}+R_k) \end{cases} \tag{24}$$

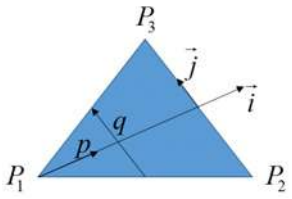

FIGURE 9. THE PARAMETRIZATION.

The subscript is the index of the vertices and $k = 1,2,3$.

- If the field point M is located at a vertex location P_k on the triangle S_i, the integral is singular.

$$(R_k, d_k, Z, N_k^1, D_k^1, N_k^t, D_k^t) = (0, R_{k+1}, 2R_{k+1}, 0, 0, 0) \quad (25)$$

Let us assume that $M = P_1$. The solution for $M = P_2$ or $M = P_3$ can be obtained by reordering the vertices. The parametrization on the triangle S_i is shown in Fig. 9. One can see that $\vec{i} = 1/2(\overrightarrow{P_1P_2} + \overrightarrow{P_1P_3})$, $\vec{j} = \overrightarrow{P_2P_3}$, $\vec{h} = \vec{i} \wedge \vec{j}$. $\overrightarrow{MP} = p\vec{i} + pq\vec{j}$ with $(p,q) \in [0,1] \times [-\frac{1}{2}, \frac{1}{2}]$. The surface integral can be written:

$$\begin{aligned} S_\sigma(M) &= \iint_{S_i} \frac{1}{p\sqrt{\vec{i}^2 + 2q\vec{i}\cdot\vec{j} + q^2\vec{j}^2}} \parallel \vec{h} \parallel pdpdq \\ &= \frac{\parallel \vec{h} \parallel}{\sqrt{\vec{j}^2}} ln(\frac{a+b+\sqrt{1+(a+b)^2}}{-a+b+\sqrt{1+(-a+b)^2}}) \end{aligned} \quad (26)$$

where $a = \frac{1}{2}\frac{\vec{j}^2}{\sqrt{\Delta}}$, $b = \frac{(\vec{i}\cdot\vec{j})}{\sqrt{\Delta}}$ and $\Delta = \vec{i}^2\vec{j}^2 - (\vec{i}\cdot\vec{j})^2$.

Line integral of term $\vec{I}_\sigma(M)$

The Line integral $\vec{I}_\sigma(M) = \oint_{C_i} MP\vec{n} \wedge \overrightarrow{dl}$ can be divided into three parts for the three edges of the triangle, $\vec{I}_\sigma(M) = \vec{I}_{\sigma P1P2}(M) + \vec{I}_{\sigma P2P3}(M) + \vec{I}_{\sigma P3P1}(M)$. Here the results are given for the line AB as a reference. Let us recall that P is located in AB. The integral which needs to be solved is

$$\vec{I}_{\sigma AB}(M) = \int_A^B MPdl\vec{k}_s \quad (27)$$

with the local coordinates $(\vec{k}_s, \vec{k}_t, \vec{k}_n)$ defined by $\vec{k}_s = \vec{k}_n \wedge \vec{k}_t$, $\vec{k}_t = \frac{\overrightarrow{AB}}{AB}$, $\vec{k}_n = \vec{n}$, $t = \frac{AP}{AB}$, $t \in [0,1]$ and $dl = ABdt$. The parametrization can be seen in Fig. 10. Using the law of cosines, one can show:

$$MP^2 = AP^2 + AM^2 - 2\overrightarrow{AP}\cdot\overrightarrow{AM} = K^2(1+q^2) \quad (28)$$

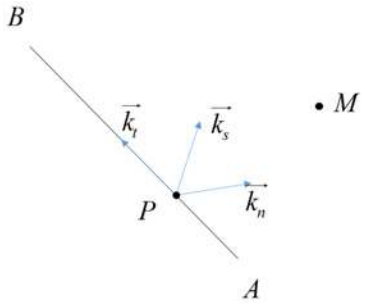

FIGURE 10. THE REFERENCE FOR LINE INTEGRAL OF SOURCE

where

$$\begin{cases} K^2 = AM^2 - (\frac{\overrightarrow{AB}\cdot\overrightarrow{AM}}{AB})^2 \\ q = \frac{1}{K}(tAB - \frac{\overrightarrow{AB}\cdot\overrightarrow{AM}}{AB}) \end{cases} \quad (29)$$

- If $K > 0$, M is not on the line AB. The integral can be solved by substitution

$$\begin{aligned} \vec{I}_{\sigma AB}(M) &= \int_{q_0}^{q_1} K\sqrt{1+q^2}dq\frac{\vec{k}_n \wedge \overrightarrow{AB}}{AB} \\ &= K^2 \int_{asinh(q_0)}^{asinh(q_1)} \sqrt{1+sinh(x)^2}cosh(x)dx\frac{\vec{k}_n \wedge \overrightarrow{AB}}{AB} \\ &= \frac{K^2}{2AB}[b-a+\frac{sinh(2b)-sinh(2a)}{2}]\vec{k}_n \wedge \overrightarrow{AB} \end{aligned} \quad (30)$$

with $a = asinh(-\frac{\overrightarrow{AB}\cdot\overrightarrow{AM}}{AB\cdot K})$, $b = asinh(\frac{AB^2 - \overrightarrow{AB}\cdot\overrightarrow{AM}}{AB\cdot K})$.

- $K = 0$, M is on the line AB

$$\begin{aligned} \vec{I}_{\sigma AB}(M) &= \int_A^B MPdl\frac{\vec{k}_n \wedge \overrightarrow{AB}}{AB} \\ &= \int_0^1 (MA + \frac{\overrightarrow{AB}\cdot\overrightarrow{AM}}{AM\cdot AB}tAB)(ABdt)\frac{\vec{k}_n \wedge \overrightarrow{AB}}{AB} \\ &= (MA + \frac{1}{2}\frac{\overrightarrow{AB}\cdot\overrightarrow{AM}}{AM})\vec{k}_n \wedge \overrightarrow{AB} \end{aligned} \quad (31)$$

Surface integral of term $S_\sigma(M)$

- For $M \notin S_i$, the integral $S_\mu(M) = \iint_{S_i} \frac{\partial}{\partial n_P}\frac{1}{MP}dS$ has an analytical solution given by Guevel [21].

$$S_\mu(M) = 2sign(Z)\sum_{k=1}^{3} \arctan(\frac{N_k^t}{D_k^t}) \quad (32)$$

where Z, N_k, D_k are defined in Eqn. 24.

- For $M \in S_i$, integral $S_\mu(M) = 0$.

Line integral of term $\vec{I}_\mu(M)$

The line integral $\vec{I}_\mu(M) = \oint_{C_i} \frac{\overrightarrow{MP}}{MP} \wedge \overrightarrow{dl}$ and $\vec{I}_\mu(M) = \vec{I}_{\mu P1P2}(M) + \vec{I}_{\mu P2P3}(M) + \vec{I}_{\mu P3P1}(M)$. Here we give the results are given for the line AB as a reference.

- For $M \notin AB$, the integral is

$$\begin{aligned} \vec{I}_{\mu AB} &= K \frac{\overrightarrow{MA} \wedge \overrightarrow{AB}}{AB} \int_{q_0}^{q_1} \frac{1}{K\sqrt{(1+q^2)}} dq \\ &= \frac{\overrightarrow{MA} \wedge \overrightarrow{AB}}{AB} [asinh(q_1) - asinh(q_0)] \end{aligned} \tag{33}$$

  The sign of $\vec{I}_{\mu AB}$ is corrected compared to Letournel's paper.
- For $M \in AB$ (which means $K = 0$), $\vec{I}_{\mu AB} = 0$.